

Training Data Augmentation for Deep Learning RF Systems

Journal Title
XX(X):1-16
©The Author(s) 2021
Reprints and permission:
sagepub.co.uk/journalsPermissions.nav
DOI: 10.1177/ToBeAssigned
www.sagepub.com/

SAGE

William H. Clark IV¹, Steven Hauser², William C. Headley¹, and Alan J. Michaels¹

Abstract

Applications of machine learning are subject to three major components that contribute to the final performance metrics. Within the category of neural networks, and deep learning specifically, the first two are the architecture for the model being trained and the training approach used. This work focuses on the third component, the data being used during training. The questions that arise are then “what is in the data” and “what within the data matters?” Looking into the Radio Frequency Machine Learning (RFML) field of Modulation Classification, the use of synthetic, captured, and augmented data are examined and compared to provide insights about the quantity and quality of the available data presented to the training routine. In general, all three data types have useful contributions to a final application, but captured data germane to the intended use case will always provide more significant information and enable the greatest performance. Despite the benefit of captured data, the difficulties that arise from collection often make the quantity of data needed to achieve peak performance impractical. This paper helps quantify the balance between real and synthetic data, offering concrete examples where training data is parametrically varied in size and source.

Keywords

RFML, simulation, augmentation, captured data, machine learning, neural networks

1 Introduction

Radio Frequency Machine Learning (RFML) is the application of machine learning to problems within the Radio Frequency (RF) domain. While machine learning is a broad term that applies to many techniques, this work looks specifically into Deep Learning (DL) within RFML. The data used during the training of the network is a fundamental component for taking a problem and developing a solution to that problem. Once a reliable training routine and a network of sufficient size have been identified, how well a trained network is able to solve the problem often comes down to the quantity and quality of the data available¹. Effectively, there are three sources of data that can be used to train networks within the RFML space, simulated or synthetic²⁻⁶¹, captured or collected^{5,6,12,17,29,31,42,48,62-81}, and augmented^{5,41,42,58,65,72}, which is a combination of the first two using domain knowledge (focus of this work), or using Generative Adversarial Networks (GAN) as performed in⁴¹. Due to the nature of the RFML data space, simulated data is inexpensive thanks to open source tool-kits like GNU Radio²⁴, where observations can be generated uniquely in parallel with the only bottleneck being the available compute resources. Comparatively, performing an Over-the-Air (OTA) collection costs many orders of magnitude greater in terms of time and money due to procurement of the hardware transceivers and having to generate data in real time rather than in parallel as is done in simulation, yet all the work done in order to simulate the data is still needed when not directly examining COTS equipment. That cost only increases once collection is moved onsite to environments of interest for acquisition of the highest quality data because robust mobile systems need to be

assembled in order to perform collects while recording and storing the vast quantities of IQ data needed for training. This is a familiar problem in other domains such as image processing, where labeled training datasets are augmented to expand the size of the datasets and improve neural network generalization performance⁸²⁻⁸⁴, such that data augmentation becomes a viable alternative and builds off a comparably smaller collected dataset. In⁵⁸, using synthetic permutations of an Additive White Gaussian Noise (AWGN) class and combining that with other classes was enough to increase the performance of their network in the Army Rapid Capabilities Office’s (RCO) Blind Signal Classification Competition with an augmentation factor of seven; i.e., adding seven augmentations per observation to the original dataset.

In order to understand the impact augmentation brings to RFML, an application space is needed without loss of generalization. Due to the widely studied problem of Automatic Modulation Classification (AMC) within RFML, the AMC problem space makes a good way to test the promise of augmentation in RFML data without having to perform a full exploratory study determining the network and training routines needed in order to perform well. From the work done on RF Fingerprinting, the identification of the transmitter device, it is known that the channel between transceivers plays an important role in what can be learned from the data⁷⁸, thus the quality of the data rises as the collection environment better resembles that of the intended application space. Additionally, not only does the environment matter, but the role of the algorithms in detecting and isolating a signal also play an important role since the imperfections in the algorithms has an impact on a network’s performance in AMC when not considered³⁸. One

arXiv:2010.00178v3 [cs.LG] 19 Nov 2020

final factor known for AMC is that for diverse waveform spaces a significant amount, $> 1M$ observations, of data is required⁴⁸. In order to better gauge augmentation, focus will be on augmenting the detection imperfection space along with varying the effective Signal-to-Noise Ratio (SNR), as these are computationally cheap augmentations rather than trying to quantify the imperfections observed in the propagation path. Here propagation path refers to any effects that deviate the signal from ideal digital representation, which include everything from the transmitter's Digital-to-Analog Converter (DAC) up to the receiver's Analog-to-Digital Converter (ADC). The detection imperfections are taken as a post processing effect imposed by the detection algorithm after the receiver's ADC. While the work in⁴⁸ does perform AMC with Over-the-Air (OTA) data collection, it does so in a relatively benign environment, therefore the work is closer to what⁷⁸ called a *static* channel, rather than a more realistic *dynamic* channel to which significantly more preprocessing was used to overcome.

This work seeks to answer several questions open in the field. First, with no first hand knowledge of the degradation of the signals to be seen, how well does a synthetically trained, validated, and tested network actually perform under real-world conditions in the field? The major investigation here is the contrast between a synthetic dataset where, through simulation, distortion is applied to the signals and compared to the field collection of data where all of the distortion is taken from the signals' propagation through the environment.

Second, what value does augmentation bring in contrast to just performing an extended capture? This question addresses the initial data collection concerns when starting a new problem or a repeat application within a new environment, which is because deep learning typically has a nonlinear relationship between performance and the number of observations in a dataset. For narrowband signals, getting another order of magnitude of examples may change the length of time running a collection from days into months of field time. In the absence of enough data, augmentation is relied upon to provide a greater observational data space, and by comparison, is relatively cheap in terms of time and effort to that of a traditional collection campaign; however, the value of one augmented observation contrasted with one collected observation in terms of performance is not well known. Further, many military spectrum access applications require modeling of channel effects that cannot be practically tested live.

The third question answered here is whether understanding the distributions of degradation sources impacts the ability of a network to achieve peak performance. That is, can a general degradation region be sufficient to allow the network to generalize over that degradation space, or will matching the distribution of a degradation prove to be more beneficial to the network's performance in that range. There are two cases to examine under this question: synthetic generation and augmentation. For the synthetic portion of this inquiry, the focus is on whether drawing parameters from the assumed degradation region, or drawing parameters from estimations extracted from the observation space allow for any change in performance of the trained network when tested against collected data. With the augmentation portion,

the question is does it matter how the degradation space is resampled in the augmented observations, for example can augmentation be performed using an assumed parameter degradation region like with the synthetic example, or should the resampling come from the collected observation space instead.

The work in this paper reinforces the results of³⁸, which show the effects of the detection and isolation algorithms should not be ignored for practical real-world applications, and when used intelligently with augmentation can improve performance. However, as shown in⁷⁸ the propagation path is a greater barrier to high fidelity synthetic data than the detection and isolation imperfections alone. The quantification of the training data required to achieve a desired level of performance in a DL RFML application will support predictive measures of data needs for other applications.

The rest of this paper is outlined as follows. In Section 2, a description of the experiment performed in this work is outlined and covers the model architecture, training routine, database used, and the AMC problem spaces being trained in. In total, three AMC problem spaces are considered, each with a different number of waveforms present in the space and consist of 3, 5, and 10 waveforms. In Section 3, the primary results from the three waveform spaces are presented and discussed in terms of the three questions outlined above, focusing on understanding how the quantity and quality of a dataset impact AMC performance. Section 4 poses open questions that this work raises for future efforts and broadens consideration to other RFML applications. And finally, in Section 5, parting thoughts and conclusion are given.

2 Experiment Setup

As the focus of this work is to examine the effects of quantity and quality of the available data to the RF problem space of AMC, the architecture for the model to be trained along with a DL training routine were identified and remain consistent for all aspects of the results shown within this work. The experiment, shown in Figure 1, consists of training a Convolutional, Long-Short Term Memory Deep Neural Network (CLDNN) for a maximum of 50 epochs through all available training data after a 90%/10% split for training and validation datasets respectively. For the case where there are 101 observations for a waveform, 91 observations per waveform are in the training dataset while 10 per waveform are in the validation dataset. A second condition for stopping is allowed for in the form of early exiting when the validation loss does not decrease for 4 epochs. A discussion for the selection of the architecture, training routine, and datasets follow.

2.1 Network Architecture

An extensive investigation of architecture was undertaken in²⁷, where different networks from the literature were compared and contrasted. The dominant network for performing AMC was found as the CLDNN, and a practical description for implementation was given in⁸⁵ with the addition of batch normalization throughout the network. From these works the network used in this experiment, as seen in Figure 2, is then a CLDNN with three 1D convolution

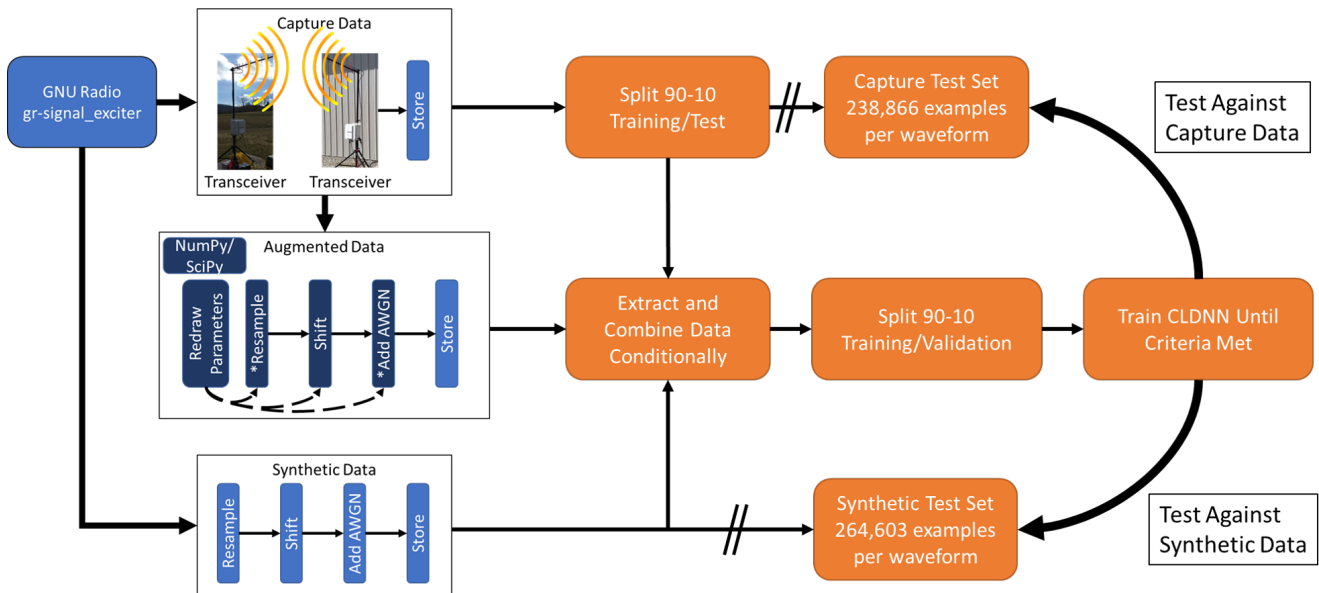


Figure 1. Experiment Configuration. At the start of each experiment, data is extracted from either a synthetic database, a capture database, and/or conditionally from an augmented database based on the extraction from the capture database. All data is then combined and split into 90%/10% training/validation datasets used to train a CLDNN network until an exit condition is met. The ‘//’ indicate a separate file has been created to better isolate the testing data from the training data.

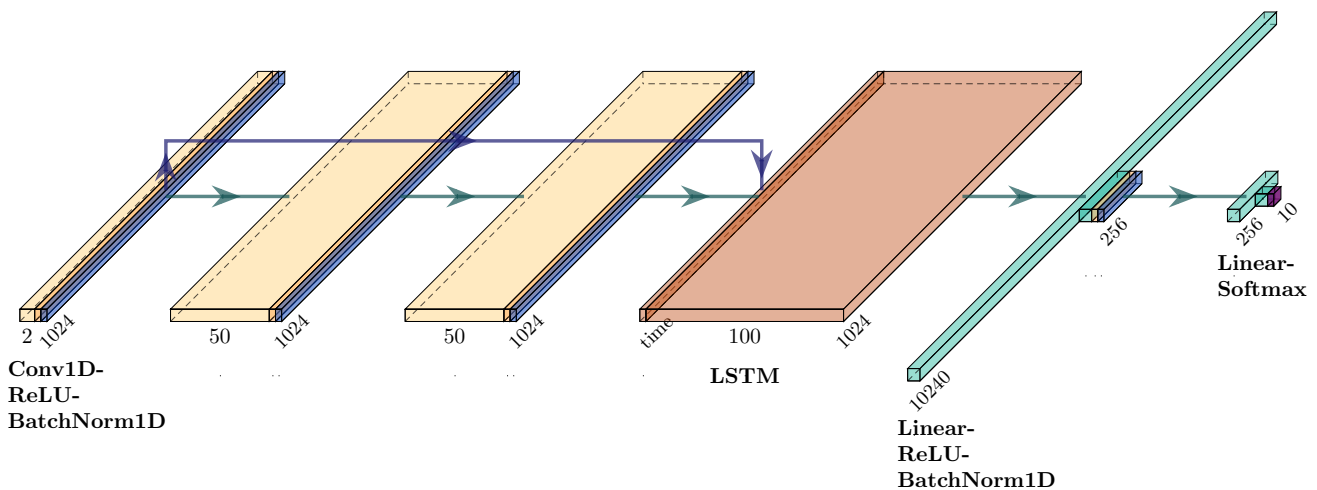


Figure 2. CLDNN Architecture for the Φ_{10} (Section 2.4) waveform dataset.

layers with 50 output channels, using a 1x8 kernel size, whose input is padded with zeros such that the output sequence is of the same length as the input, followed by a Rectified-Linear Unit (ReLU) activation, and a 1D batch normalization layer. The output of the first and third such layers are then concatenated along the channel dimension and passed through a single LSTM layer such that the channels are taken as the features while the time sequence is fed through the LSTM’s memory structure. For simplicity, the LSTM has a hidden size equal to the number of classes being used in the problem. The output of the LSTM is then flattened and passed through a linear layer with 256 output nodes with a ReLU Activation and 1D Batch Normalization. The final batch normalization layer is then connected to the final linear layer with the number of outputs equal to the number of classes with a Softmax Activation. This network structure was chosen as the baseline for the experiment for two main reasons, the first being the high performance seen

in²⁷, with the second being that the convergence time with the training routine given next was shown to be quick in terms of epochs in⁸⁵.

2.2 Training Routine

The CLDNN network is trained consistently for all data quantities and qualities. As discussed next, the dataset for each experiment is selected, and then split 90/10% into training and validation datasets respectively. These two datasets are then distinct for that experiment and model trained. The data is then processed in batches consisting of 1500 total observations. Using the default Adam optimizer⁸⁶ within PyTorch with Cross Entropy Loss, the network is allowed to continually train until 4 epochs have passed without any improvement in the validation loss metric or until 50 epochs have been processed.

The goal of this training routine is to minimize the Cross Entropy Loss of the validation dataset consistently as it

processes from one epoch to the next. When the consistent decreasing of the validation loss is not observed after four contiguous passes through the training dataset, the training routine takes this as the model has begun overfitting to the dataset and recovers the set of weights that achieved the lowest validation loss value.

While this training routine doesn't allow for significant deviation in the event a local minimum is found, it is chosen for the ideal properties of having a quick consistent goal and a limited processing window within which to achieve said goal. In order to quantify the value data brings to a network, hundreds to thousands of networks need to be trained; allowing a more lenient training routine would only extend the total time taken to train a single model. The approach was decided on taking into consideration the total processing time needed to perform the investigation.

2.3 The Dataset

The database being used in this investigation was made from live collection of numerous waveforms at Virginia Tech's Kentland Farms over the course of 4 months in 2018 using two weather enclosed software-defined radios (shown in Figure 1). The database consists of multiple waveforms of varying duration and quality. Based on the metadata available, the data was filtered to only select observations whose Signal-to-Noise Ratio (SNR) was estimated to be above -10 dB. Additionally, due to the nature of hardware collections and an active environment, observations that were found to have irregular sample values and were filtered out from the dataset. The data was then segmented such that observations of 1024 samples could be extracted in a continuous fashion with no two observations being contiguous outside of 1024 samples. In other terms, given one observation starting at sample 0, the next observation could not start until sample 2048 assuming there are at least 3072 samples available in that record. The final filter placed on the data left all waveforms evenly balanced in terms of available observation counts, resulting in 2,388,667 total observations for each waveform class considered. Of the data that remained, the detector imperfections that were estimated showed that the SNR was between -10 and 80 dB, with the majority of the data being below 20dB. The estimated Frequency Offsets (FO) were found to be bounded by $\pm 20\%$ of the receiver's sampling rate though heavily concentrated between $\pm 5\%$. The Sample Rate Mismatches (SRM) found signals in the range of 2-32 times that of the Nyquist rate, though roughly twice as likely to be between 2-8 as between 8-32. In order to better make use of the estimated distributions of the captured data, a joint Kernel Density Estimate (KDE) was performed per modulation on the imperfections of SNR, FO, and SRM to be used while augmenting and synthetically generating datasets. Table 1 provides an overview for the datasets used in this work.

2.3.1 The Capture Dataset All the observations in the dataset described above are then split into a general training set (Ω_C) and a test set (Ω_{TC}) against which all results will be compared. The training/testing split is 90/10% consisting of 2,149,801 and 238,866 observations per class respectively. As part of the investigation, the number of observations

Table 1. Datasets

| Training | | |
|---------------|------------------------------|---|
| Symbol | Source | Description |
| Ω_C | Capture | Consists of only capture examples |
| Ω_{SS} | Synthetic | Consists of simulated examples using an assumed synthetic distribution |
| Ω_{AS} | Capture + Synth Augmentation | Consists of capture examples and augmentations using the synthetic distributions |
| Ω_{SK} | Synthetic using KDE | Consists of simulated examples using the KDE of the capture dataset |
| Ω_{AK} | Capture + KDE Augmentation | Consists of capture examples and augmentations using the KDE of the capture dataset |
| Testing | | |
| Ω_{TC} | Capture | Consists of only capture examples |
| Ω_{TS} | Synthetic | Consists of simulated examples using an assumed synthetic distribution |

drawn from the training set varies across iterations, but every trained model is tested against the full Ω_{TC} .

2.3.2 The Augmented Dataset Additionally, there are other datasets that can be used while training consisting of captured data. The first is an augmented dataset that is linked to the capture training set and, for every observation, 10 augmentations are made. The data drawn from the augmented dataset is conditionally linked in such a way that only augmentations of data selected from the capture training dataset will be available to be drawn, and then when the augmentation factor is less than 10, which exact augmentation is drawn is left to random uniform sampling. There are two distinct augmented datasets to understand what effect, if any, the distribution of parameters has on the performance during training.

The first augmented dataset takes on a range of parameters given as an expected performance range of the capture data prior to performing any capture. The signals are augmented in such a way that the SNR is uniformly drawn from the range of 0-20dB, the FO is taken uniformly in the range of -10% - 10% of the sampling rate, and the SRM is taken to be uniform in the range of 2-8 times that of the Nyquist rate for the captured signals. Given the available metadata and the observations of 1024 samples, any time a random value is drawn that cannot be achieved, for example a signal with an SNR value of 5dB being augmented to a signal with an SNR of 10dB, the augmentation is nulled and whatever the current estimate is holds. Likewise, SRM augmentation that requires decimation reducing the number of samples below

Table 2. Waveform Spaces

| Group | Waveforms |
|-------------|---|
| Φ_3 | BPSK, QPSK, Noise |
| Φ_5 | BPSK, QPSK, QAM16, QAM64, Noise |
| Φ_{10} | BPSK, QPSK, QAM16, QAM64, BFSK, GMSK, AM-DSB, FM-NB, GBFSK, Noise |

the desired 1024 observation length is nulled. This dataset is the Ω_{AS} dataset, and the parameter space is drawn from three independent distributions using NumPy.

The second augmentation dataset makes use of a Gaussian joint kernel density estimate (KDE), using SciPy, of the available data per captured waveform and uses a random draw from that joint estimate to perform the augmentation. This dataset is the Ω_{AK} dataset. In this way, the investigation can contrast the value of data analysis on the captured data with regard to augmentation or whether a general blind practical range will suffice.

2.3.3 The Synthetic Dataset The final two datasets consist of simulated synthetic data for the waveforms under test. Using the same distribution assumptions for the SNR, FO, and SRM as the Ω_{AS} dataset, the synthetic dataset randomly generates observations for each waveform to be used during training, Ω_{SS} . A second synthetic training set is used under the assumption that better metrics are known for SNR, FO, and SRM based on the targeted detection routine in place on the observer device and draws the parameters from the KDE discussed with the Ω_{AK} dataset; the Ω_{SK} dataset. This approach can help quantify the value of real world data that undergoes true transceiver and channel degradation that is not as easily replicated through simulation. Additionally, a single testing dataset, Ω_{TS} , is created using the blind distributions as a means for comparing what a purely synthetic test set would say about the performance of a trained model to that of captured data from the field.

2.4 Waveform Space

The waveforms selected from those available in the data consist of 3, 5, and 10 classes denoted by Φ_3 , Φ_5 , and Φ_{10} , respectively. The waveforms associated with each space are provided in Table 2. By having three different dimensions for the class size, the work is able to examine any differences that data quantity might have with regard to the difficulty of the problem. The two smaller subsets are chosen due to the frequent usage in traditional feature based approaches⁸⁷.

3 Analysis

The results presented in this section are aimed at answering each of the three research questions posed previously. In doing so, the overall analyses employ Monte Carlo ensembles that consider relative performance against synthetic (Ω_{TS}) and captured (Ω_{TC}) test datasets, and ultimately analysis of AMC application accuracy as a function of the quality and quantity of data provided during training.

3.1 Synthetic Performance in the Field

We start the analysis with the first major question in this work; for a given synthetically trained network, how well does the network perform when applied to real-world data from the field? To answer this question, three different waveform spaces, $\{\Phi_3, \Phi_5, \Phi_{10}\}$, are examined with regard to the dataset source used while undergoing training. Each trained model is then evaluated on both the synthetic and the capture test sets, $\{\Omega_{TS}, \Omega_{TC}\}$. Plotting the accuracy of the Ω_{TC} against the accuracy of the Ω_{TS} in Figures 3-5, the overall performance can be seen for the waveform spaces $\{\Phi_3, \Phi_5, \Phi_{10}\}$ respectively. For each plot, a vertical and horizontal black solid line, without markers, are used to indicate random guessing along each axis, with a third diagonal line indicating where performance would be equivalent across the two test sets. The trained networks are then represented with different markers representing different dataset sources used during training.

In terms of an ideal performance, non-filled markers should be concentrated in the top right corner of each plot, indicating high accuracy on both the Ω_{TC} and Ω_{TS} datasets, which can be used as an indication that the nuisance parameter space in the capture data that is not being modeled in the synthetic data has been well generalized over. Instead, the plots show that for models trained from a dataset that relies on either synthetic (markers triangle and pentagram) or capture (markers square, circle, and diamond) data that the model is then biased more toward better performance against an alike test set; Ω_{TC} is best performed on by captured and augmented datasets, ($\Omega_C, \Omega_{AK}, \Omega_{AS}$), while the Ω_{TS} is best performed on by the synthetic datasets, (Ω_{SS}, Ω_{SK}).

While this bias for alike datasets intuitively makes sense, there are some unique outcomes that are not obvious. There are grayed out areas marked as outliers, which are results that failed to converge to a performance using the constraint

$$\text{Lower Bound} = \max(\alpha_{\Omega_{C||S}}) \mid \alpha_{\Omega_{C||S}} < \frac{2}{|\Phi_X|}. \quad (1)$$

Here any accuracy, α , that is less than or equal to the lower bound is treated as an outlier and excluded from the analyses within this paper, while X is used as the waveform space indicator. This filter corresponds to models that did not perform better than [44.05%, 24.36%, 11.13%] from datasets $\{\Omega_C, \Omega_{AK}, \Omega_{AS}\}$ and [61.25%, 38.91%, 18.14%] from datasets $\{\Omega_{SS}, \Omega_{SK}\}$ set in the waveform spaces $\{\Phi_3, \Phi_5, \Phi_{10}\}$ respectively.

Observing the figures for the synthetic trained datasets (Ω_{SS} : triangle and Ω_{SK} : pentagram markers) on the performance comparison show that the synthetic data is very easily learned when tested on Ω_{TS} , but generally fails to do better than twice that of random guessing on Ω_{TC} . Table 3 shows the relational change in performance on both Ω_{TS} and Ω_{TC} when contrasting the two synthetic datasets. Contrasting the average accuracy as a ratio, $\overline{\alpha_{\Omega_{SK}}}/\overline{\alpha_{\Omega_{SS}}}$, there is a marginal loss in performance on the smallest waveform space, Φ_3 , when using the synthetic data created with the KDE, while the KDE drawn synthetic data performs a little better on average with Ω_{TC} than the non-KDE drawn synthetic data; using Welch's two-sample t-test⁸⁸, the significance of such improvement is minimal. By contrast, the decrease in average accuracy on Ω_{TS} and the increase

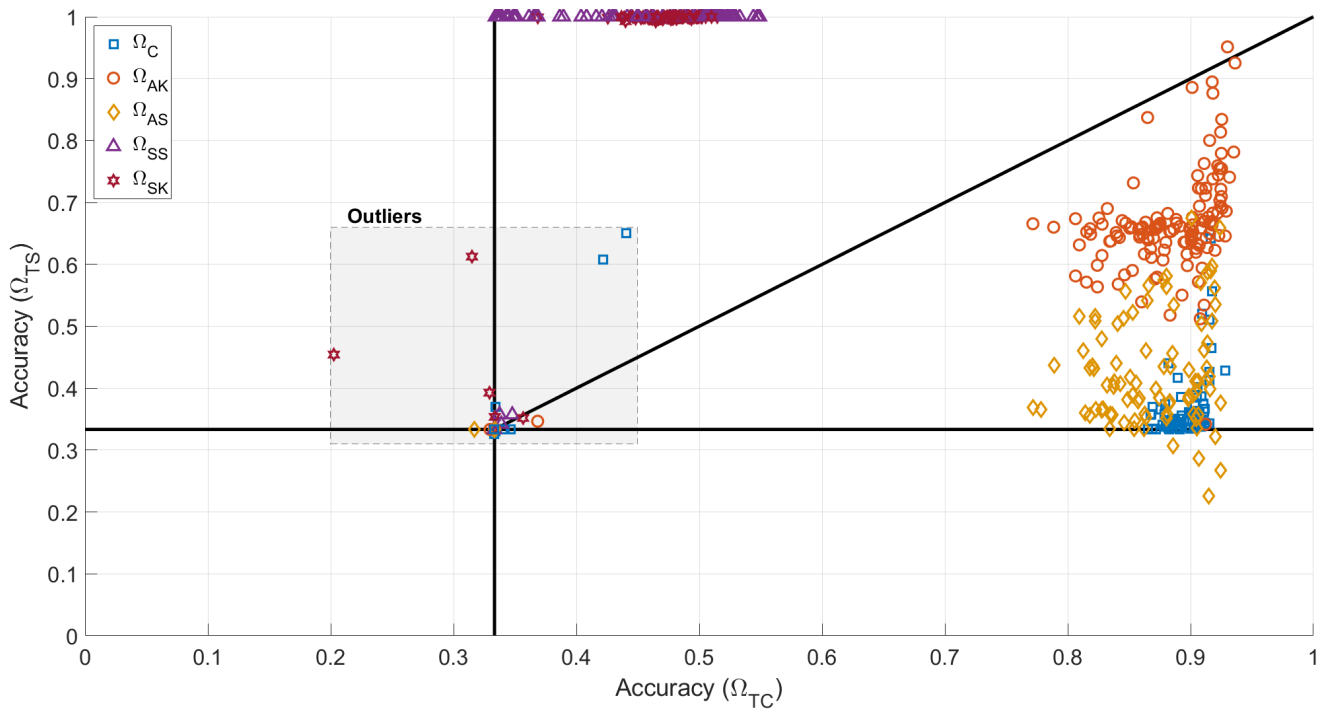


Figure 3. Performance of the five datasets on the Φ_3 waveform space contrasting the performance observed on the synthetic (Ω_{TS}) and capture (Ω_{TC}) test sets. While ideal performance is in the top right corner, an acceptable performance is to the right in general for real-world performance. While high performance is found on data similar to their respective training datasets, neither synthetic nor captured data performs well on the other. Through augmentation of captured, a greater performance is observed on the synthetic data as a result indicating better generalization over the full parameter space.

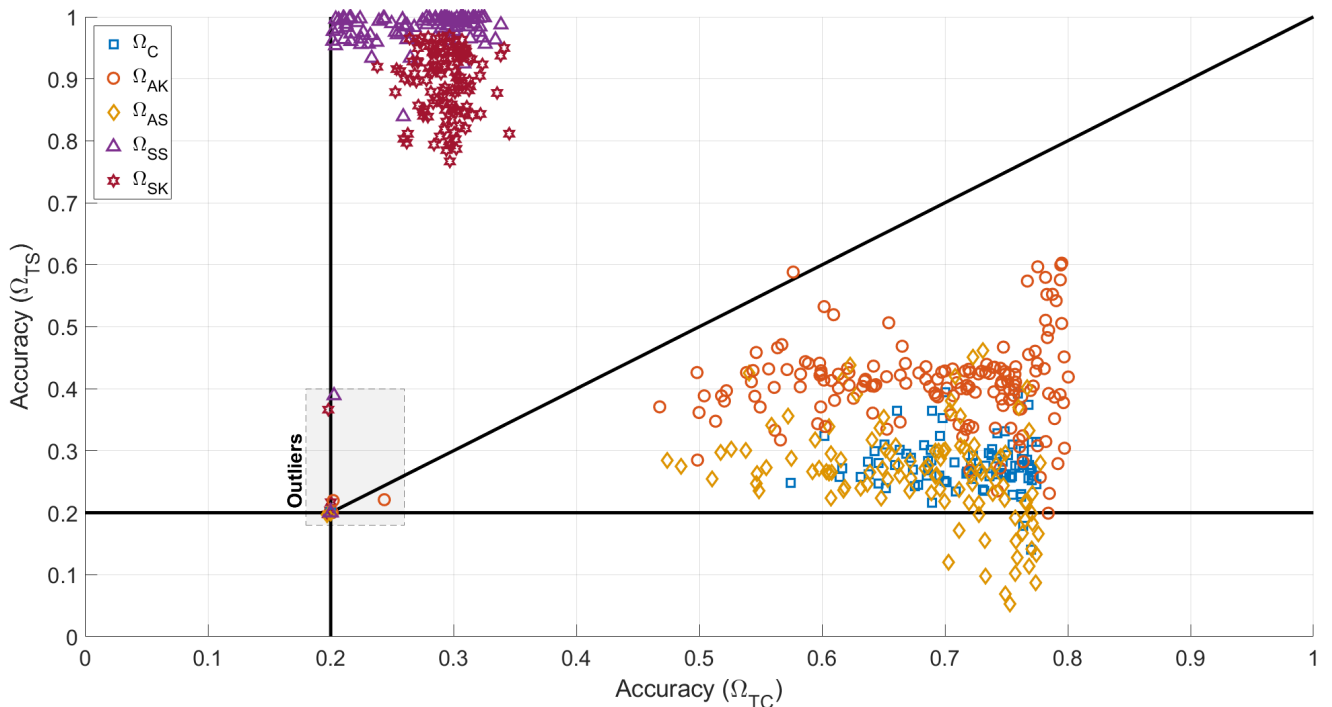


Figure 4. Performance of the five datasets on the Φ_5 waveform space contrasting the performance observed on the synthetic (Ω_{TS}) and capture (Ω_{TC}) test sets. While ideal performance is in the top right corner, an acceptable performance is to the right in general for real-world performance. In contrast to Figure 3 the generalization over the parameter space is less pronounced when using augmented data in the same quantity range per waveform; however, the augmented dataset with knowledge of the parameter space (Ω_{AK}) still provides improved generalization, while augmentation without such knowledge ends up reducing generalization instead.

in average accuracy on Ω_{TC} for Φ_5 show a much greater significance indicating that the use of the imperfections from the intended environment can improve the fidelity of

synthetic datasets. However, the improvement on the capture test set is lost as the waveform space continues to grow with Φ_{10} . In general, there is a slight possibility that creating

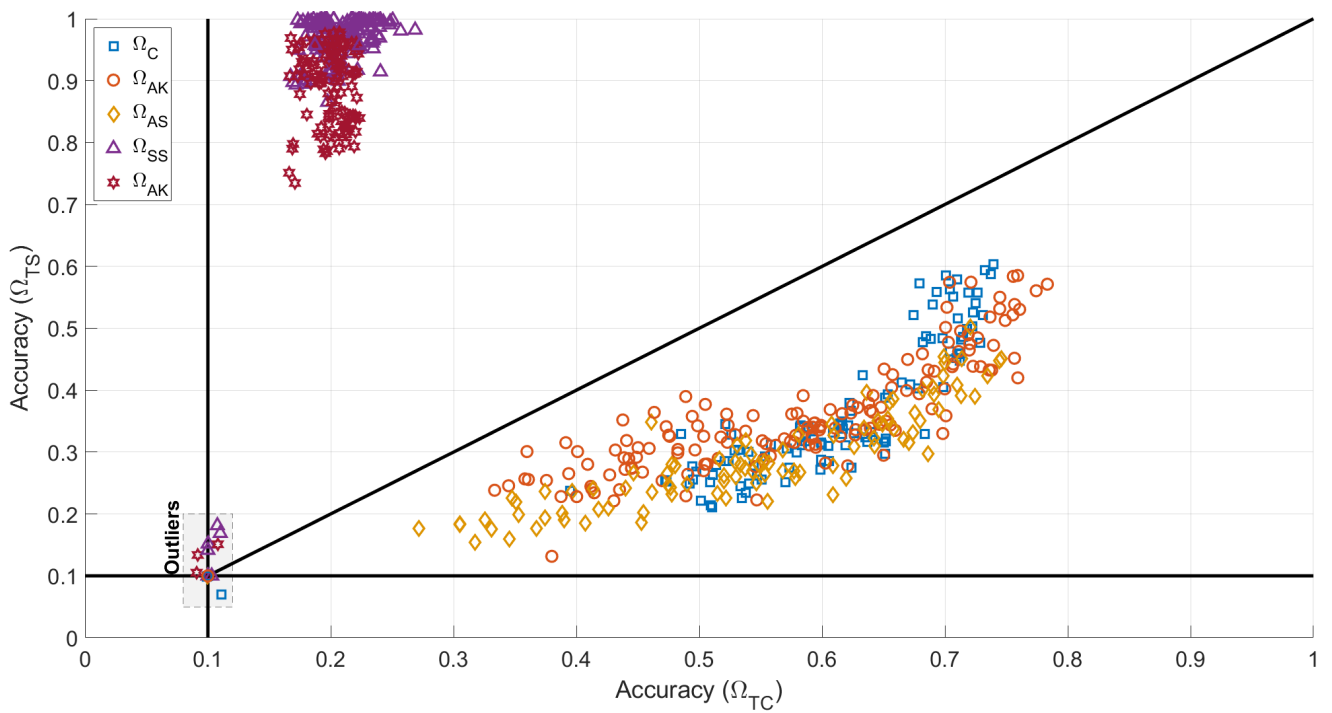


Figure 5. Performance of the five datasets on the Φ_{10} waveform space contrasting the performance observed on the synthetic (Ω_{TS}) and capture (Ω_{TC}) test sets. While ideal performance is in the top right corner, an acceptable performance is to the right in general for real-world performance. In contrast to Figures 3 and 4 the generalization observed through augmentation is only observable at low accuracies on Ω_{TC} and becomes negligible as accuracy increases. As the difficulty increases, the improved generalization that can be observed with augmented data within lower difficulty problems disappears in higher difficulty problems when constrained to the same quantity/quality availability during training. It is unclear whether quantity or quality directly play a role of significance in this observation.

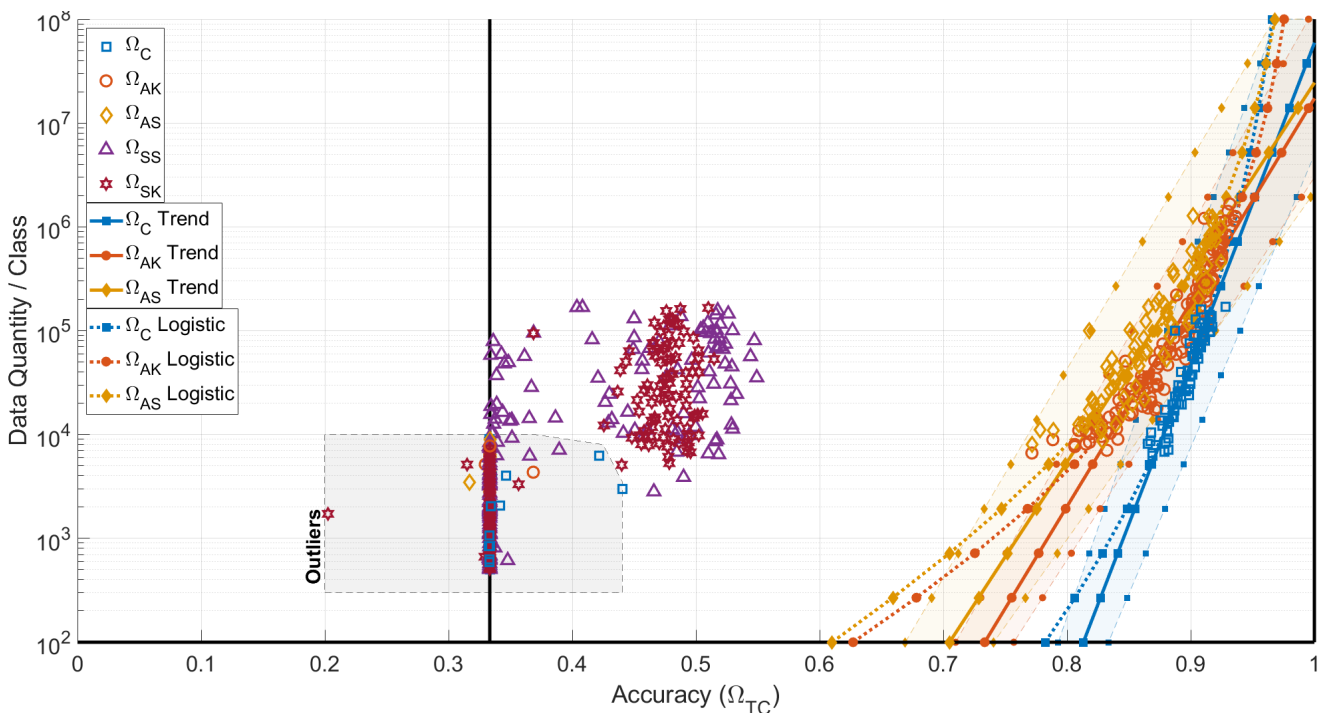


Figure 6. Performance of models trained using the five datasets on the Φ_3 waveform space. Solid lines represent the trend in terms of examples per class that are needed to achieve a given accuracy on the capture test data, while the shaded regions between dashed lines with the matching markers indicate a 95% confidence region for that trend. Synthetic datasets are omitted from the trend analysis as no significant trend was observed from these datasets. Trends are derived with outliers removed. The further right the trend line, the higher the quality of data. Additionally, a dotted line is fit to the data using a logistic regression with the assumption that 100% accuracy is possible given the asymptotic curve perceived in the data and the impossibility of performance greater than 100% accuracy.

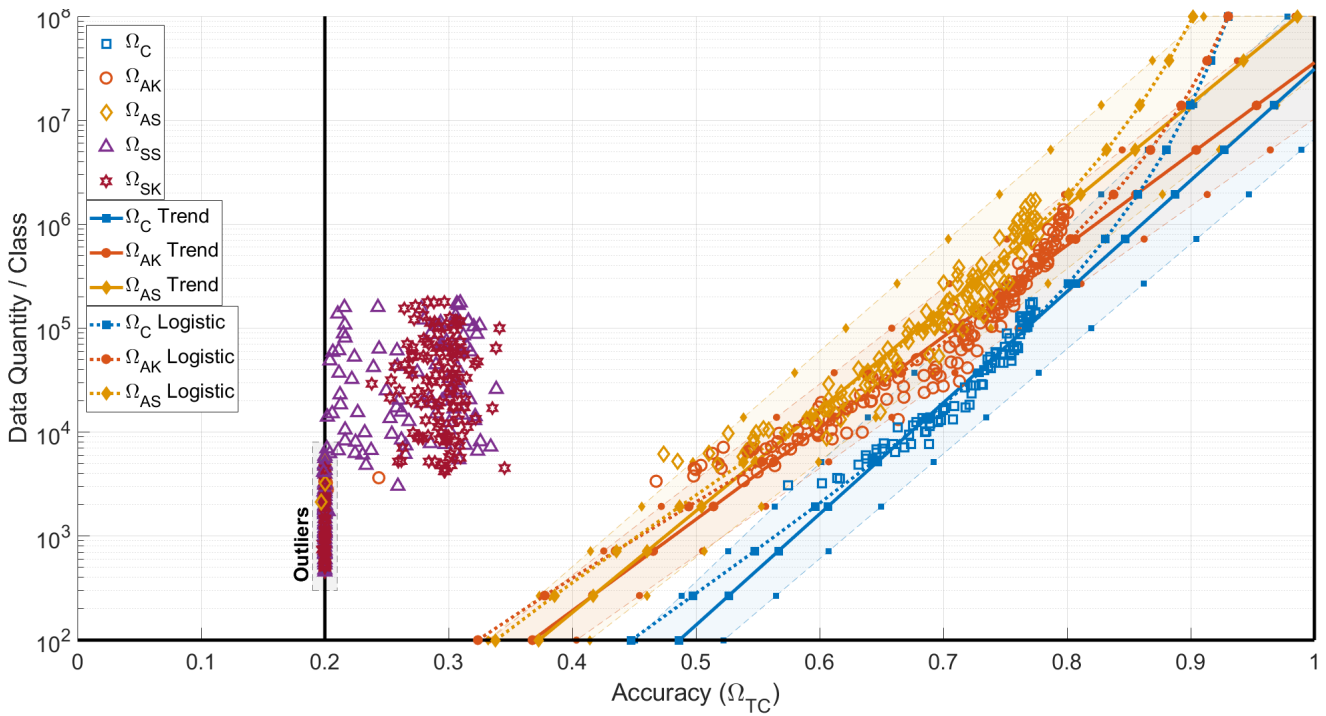


Figure 7. Performance of models trained using the five datasets on the Φ_5 waveform space. Solid lines represent the trend in terms of examples per class that are needed to achieve a given accuracy on the capture test data, while the shaded regions between dashed lines with the matching markers indicate a 95% confidence region for that trend. Synthetic datasets are omitted from the trend analysis as no significant trend was observed from these datasets. Trends are derived with outliers removed. The further right the trend line, the higher the quality of data. Additionally, a dotted line is fit to the data using a logistic regression with the assumption that 100% accuracy is possible given the asymptotic curve perceived in the data and the impossibility of performance greater than 100% accuracy.

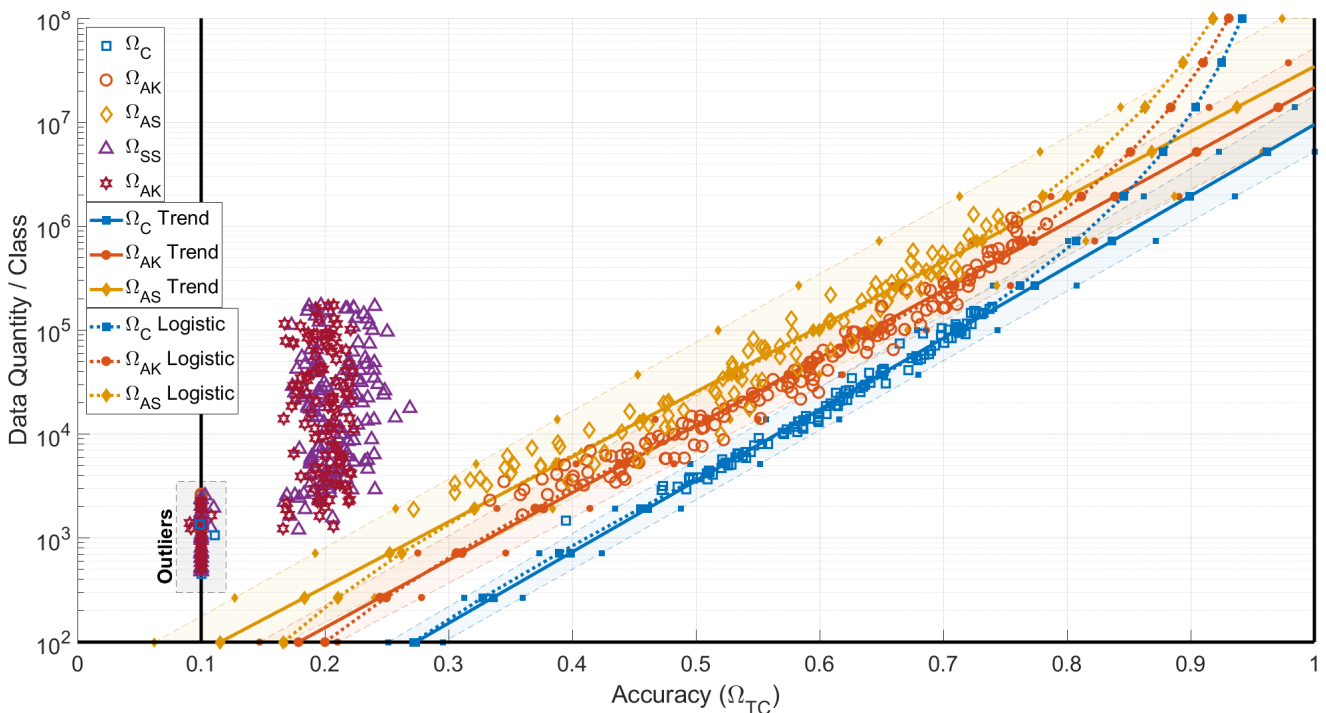


Figure 8. Performance of models trained using the five datasets on the Φ_{10} waveform space. Solid lines represent the trend in terms of examples per class that are needed to achieve a given accuracy on the capture test data, while the shaded regions between dashed lines with the matching markers indicate a 95% confidence region for that trend. Synthetic datasets are omitted from the trend analysis as no significant trend was observed from these datasets. Trends are derived with outliers removed. The further right the trend line, the higher the quality of data. Additionally, a dotted line is fit to the data using a logistic regression with the assumption that 100% accuracy is possible given the asymptotic curve perceived in the data and the impossibility of performance greater than 100% accuracy.

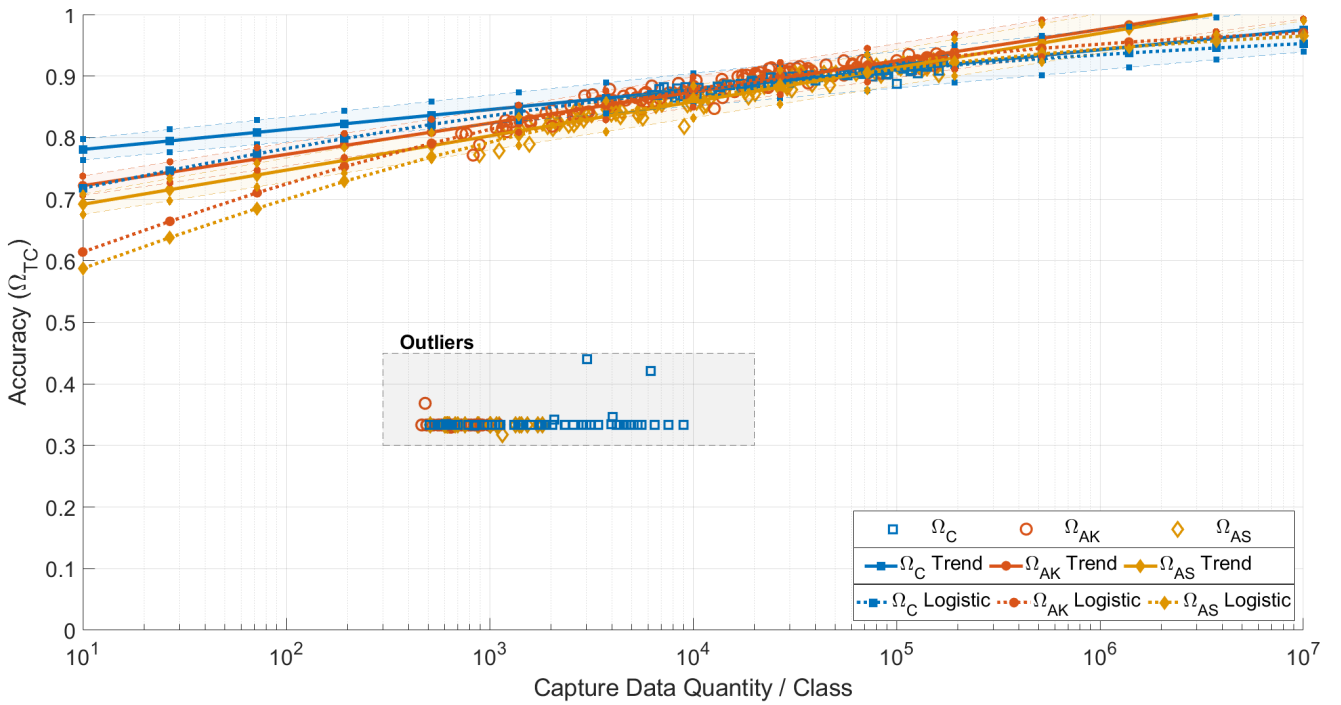


Figure 9. Performance of models trained using the three capture datasets on the Φ_3 waveform space. Solid lines represent the trend in terms of examples per class that are needed from Ω_C to achieve a given accuracy on the capture test data with or without any augmentation, while the shaded regions between dashed lines with the matching markers indicate a 95% confidence region for that trend. Trends are derived with outliers removed. The higher the trend line, the higher the quality of the dataset. The dotted lines represent a log-logistic regression to account for the asymptotic curvature observed in the results. Under both sets of regression, the models using dataset Ω_{AK} exhibit a higher quality data with increasing data quantity.

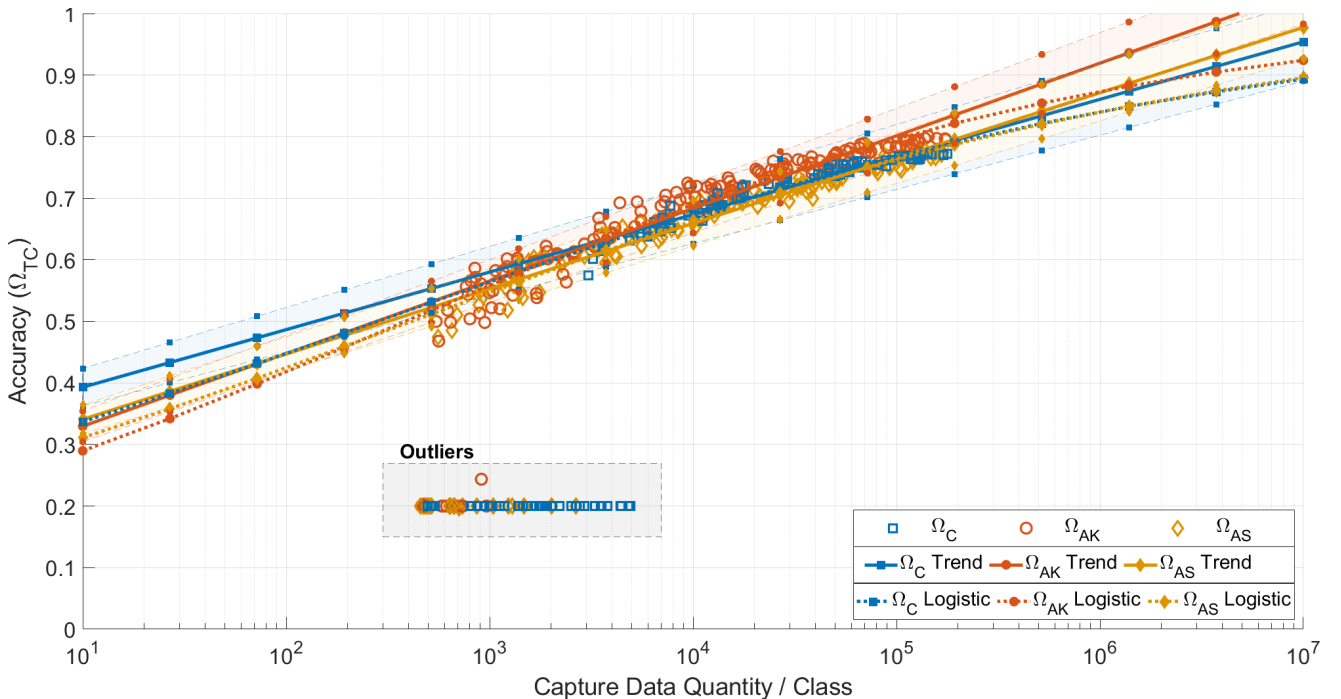


Figure 10. Performance of models trained using the three capture datasets on the Φ_5 waveform space. Solid lines represent the trend in terms of examples per class that are needed from Ω_C to achieve a given accuracy on the capture test data with or without any augmentation, while the shaded regions between dashed lines with the matching markers indicate a 95% confidence region for that trend. Trends are derived with outliers removed. The higher the trend line, the higher the quality of the dataset. The dotted lines represent a log-logistic regression to account for the asymptotic curvature observed in the results. Under both sets of regression, the models using dataset Ω_{AK} exhibit a higher quality data with increasing data quantity.

synthetic data that only considers the detector imperfections can be of high enough fidelity to train as the number of

synthetic examples increases by many order of magnitudes, but overall these results show that modeling only the detector

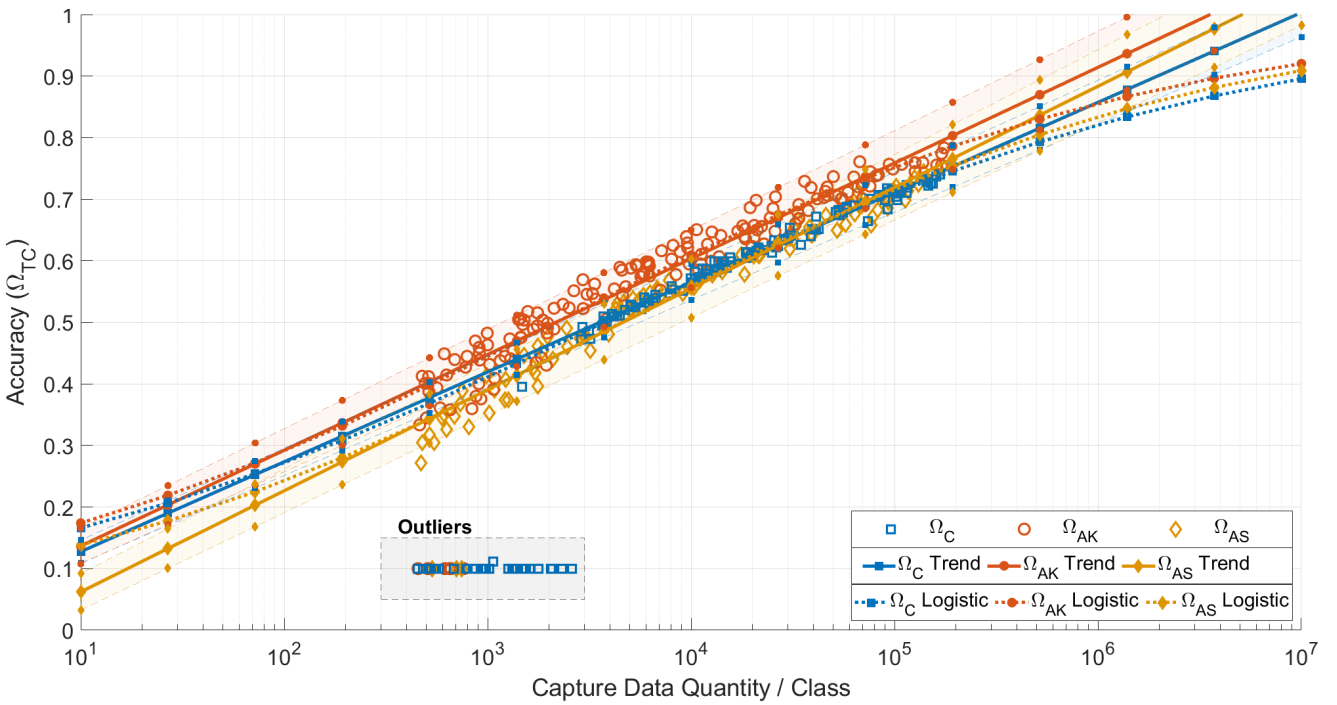


Figure 11. Performance of models trained using the three capture datasets on the Φ_{10} waveform space. Solid lines represent the trend in terms of examples per class that are needed from Ω_C to achieve a given accuracy on the capture test data with or without any augmentation, while the shaded regions between dashed lines with the matching markers indicate a 95% confidence region for that trend. Trends are derived with outliers removed. The higher the trend line, the higher the quality of the dataset. The dotted lines represent a log-logistic regression to account for the asymptotic curvature observed in the results. Under both sets of regression, the models using dataset Ω_{AK} exhibit a higher quality data with increasing data quantity.

Table 3. Test Accuracy's Observed Response to Synthetic Datasets Ω_{SS} and Ω_{SK} . Examines the significance of where the detection imperfections are drawn from compared to what is tested against. Smaller values (< 0.05) indicate larger significance of where the simulation degradation is drawn from. p-values found using Welch's two sample t-test.

| Waveform Space | Average Accuracy Ratio | | p-values | |
|----------------|-----------------------------------|---------------|---------------|---------------|
| | $\frac{\Omega_{SK}}{\Omega_{SS}}$ | | Ω_{TS} | Ω_{TC} |
| | Ω_{TS} | Ω_{TC} | | |
| Φ_3 | 0.998 | 1.05 | $1.2196e-10$ | $3.9351e-3$ |
| Φ_5 | 0.910 | 1.08 | $1.3715e-35$ | $5.6249e-6$ |
| Φ_{10} | 0.921 | 0.954 | $1.9963e-23$ | $2.6340e-5$ |

imperfections while ignoring the propagation path is not significant enough to properly train a system heading to the field. This result answers the first question of when given a network trained and tested in the synthetic space, that network will not perform well in a real system without a much higher fidelity simulated dataset. Additional work is still needed to determine at what threshold simulated data can be considered high enough fidelity when designing and developing a deployable system. In all likelihood, finding that threshold is going to be very dependent on the target operating environment. This includes how much is known about the transceiver to transceiver propagation path, which includes everything from the transmitter's DAC through the receiver's ADC, and any effects of the detection and isolation stages inherent to that receiver.

Table 4. Log-Linear fits, $qty = 10^{\left(\frac{\alpha - p_2}{p_1}\right)}$, for data presented in Figures 6-8.

| Dataset | Waveform Space (p_1, p_2) | |
|---------------|-----------------------------|-------------------|
| | Φ_3 | Φ_5 |
| Ω_C | 0.03237, 0.7485 | 0.09351, 0.2995 |
| Ω_{AK} | 0.05091, 0.6317 | 0.1138, 0.1402 |
| Ω_{AS} | 0.05476, 0.5955 | 0.1022, 0.1686 |
| Ω_{SS} | 0.04183, 0.2656 | 0.01537, 0.2030 |
| Ω_{SK} | 0.002380, 0.4650 | -0.002029, 0.3019 |
| | Φ_{10} | |
| Ω_C | 0.1459, -0.01837 | |
| Ω_{AK} | 0.1540, -0.1294 | |
| Ω_{AS} | 0.1598, -0.2043 | |
| Ω_{SS} | 0.008621, 0.1721 | |
| Ω_{SK} | -0.001438, 0.2050 | |

3.2 Value of Augmentation

To start answering the second question of what value does augmentation bring to the problem, the attention shifts focus proximity of the models trained with Ω_C , Ω_{AK} , and Ω_{AS} datasets (square, circle, and diamond markers, respectively) to that of the diagonal line where there are performance generalizations that become less pronounced as the waveform space grows. For the capture dataset models, the clusters show that Ω_{AK} typically achieves better performance on Ω_{TS} than both Ω_C and Ω_{AS} , indicating that the degradation encountered from imperfect

detector estimation when accounted for in augmentation, does help the network better generalize over the nuisance parameters present in the capture data. Conversely, and more surprisingly, augmenting the dataset with the assumed synthetic range actually made the performance on the Ω_{TS} worse than without the augmentation. One conclusion that can be drawn from this is that the degradation encountered between one transceiver’s DAC to another transceiver’s ADC has a greater effect on performance than the degradation caused by the detection algorithm’s imperfections, assuming detection and isolation is achieved, and that simply redrawing the parameters occurred by one detection routine for another detection routine will not be sufficient without taking into account the propagation degradation on the path between the DAC and ADC in this new environment. Such refinements will become more important as RFML systems begin to incorporate learned behaviors that have been trained with and transferred from another node.

Figures 6-8 show the relationship between the achieved performance on Ω_{TC} of each individually trained network on the x-axis, with the y-axis corresponding to the total number of uniquely stored observations available during the training of the network. By looking at the relation between accuracy achieved and total data per class used during the training, two important pieces of information can be extracted. First, the trend lines further to the right for a given total quantity exhibit a higher quality within the data, because a better performance is achievable. Using this, the quality of data decreases in the following order of the capture datasets across all examined waveform spaces: Ω_C , Ω_{AK} , Ω_{AS} . Second, assuming the log-linear trend holds, as shown in Table 4, without an asymptotic bound on accuracy (an asymptotic bound should be expected, and is given with the dotted lines), a forecast can be made on just how much data of each type is required in order to achieve ideal performance, and these quantity values are shown in Table 5, with the total continuous capture time required to perform such a capture as has been done for this dataset for each waveform space is given in Table 6 in terms of days. As the trends are not consistent across all waveform spaces, also plotted is the 95% confidence region around those trends in shaded regions bounded by dashed lines with the same marker. However, assuming that the trends would be consistent given enough observations, the general results align well with intuition in that data captured directly from the test environment is of highest quality and needs the least number of observations to achieve a target performance for the given model architecture and training routine. Second to the captured data, augmentation of data to match the nuisance parameter distributions from the test environment provides the next highest quality data for training followed by naive augmentation that doesn’t consider the full nuisance parameter distributions. Coming in last, by many orders of magnitude, is synthetic data that only considers detection imperfections while simulating the waveform spaces.

Instead, using the log-logistic parametric fits showing the parameters in Table 7 results in the observation quantities in Table 8 in order to achieve a 95% accuracy in the problem space, given that 100% accuracy would require an infinite quantity of data. This results in the more likely capture

Table 5. Quantity of examples per class needed to achieve 100% accuracy for each dataset source and waveform space. Extrapolated from linear trends in Figures 6-8. Assuming no asymptotic limit.

| Dataset | Waveform Space | | |
|---------------|----------------|----------|-------------|
| | Φ_3 | Φ_5 | Φ_{10} |
| Ω_C | 58.9e6 | 31.0e6 | 9.5e6 |
| Ω_{AK} | 17.2e6 | 35.8e6 | 21.5e6 |
| Ω_{AS} | 24.3e6 | 135.5e6 | 34.3e6 |

Table 6. Quantifying the duration of a continuous capture, with no down time needed, in order to capture all data required to fulfill the Ω_C requirement for each waveform space assuming a 40kHz sampling rate of a 5kHz baud rate signal in Days. Assuming no asymptotic limit.

| Dataset | Waveform Space | | |
|------------|----------------|----------|-------------|
| | Φ_3 | Φ_5 | Φ_{10} |
| Ω_C | 104.7 | 91.7 | 56.4 |

Table 7. Log-Logistic fits, $q_{ty} = 10^{-(\log(\frac{1-\alpha}{\alpha})/p_1 - p_2)}$, for data presented in Figures 6-8.

| Dataset | Waveform Space (p_1, p_2) | |
|---------------|-------------------------------|---------------|
| | Φ_3 | Φ_5 |
| Ω_C | 0.3452, -1.705 | 0.4674, 2.449 |
| Ω_{AK} | 0.5275, 1.015 | 0.5548, 3.328 |
| Ω_{AS} | 0.4944, 1.094 | 0.4821, 3.393 |
| | Φ_{10} | |
| Ω_C | 0.6274, 3.573 | |
| Ω_{AK} | 0.6641, 4.087 | |
| Ω_{AS} | 0.6714, 4.399 | |

Table 8. Quantity of examples per class needed to achieve 95% accuracy for each dataset source and waveform space. Extrapolated from logistic fit in Figures 6-8.

| Dataset | Waveform Space | | |
|---------------|----------------|----------|-------------|
| | Φ_3 | Φ_5 | Φ_{10} |
| Ω_C | 6.7e6 | 560.4e6 | 184.5e6 |
| Ω_{AK} | 3.9e6 | 431.7e6 | 331.6e6 |
| Ω_{AS} | 11.2e6 | 3169.8e6 | 609.1e6 |

durations shown in Table 9. These results show that for the smallest waveform space an order of magnitude less capture duration can be performed for giving up the 5% accuracy, whereas for the larger waveform spaces roughly 20 times longer capture duration will be needed even while giving up that 5% performance. One more note is that the logistic regression presumes that 100% accuracy is an asymptotically achievable feat, while it is more likely that given the model and training style that the peak performance achievable would be less than 100%.

One question that naturally follows this quality comparison of the datasets is then if augmented data is of lower quality, then why not just focus on getting more captured data? The primary reason for relying on augmentation is cost, both in terms of time and money. In terms of time, the capture dataset was collected over a 4-month window in 2018, while

Table 9. Quantifying the duration of a continuous capture, with no down time needed, in order to capture all data required to fulfill the 95% accuracy requirement using dataset Ω_C for each waveform space assuming a 40kHz sampling rate of a 5kHz baud rate signal in Days.

| Dataset | Waveform Space | | |
|------------|----------------|----------|-------------|
| | Φ_3 | Φ_5 | Φ_{10} |
| Ω_C | 11.9 | 1660.7 | 1093.4 |

the augmented datasets were generated over the course of 2-4 days each and contain an order of magnitude more observations per dataset. For full comparison, the synthetic datasets were generated over the course of 7 days for each dataset and are of the same order of magnitude as the captured data. One contributing factor for the increased generation time of the synthetic data was the design decision of extracting only one observation per execution of GNU Radio flowgraph, rather than extracting many observations from a single execution, which was done to decrease any dependence between observations within the dataset. The second cost is the monetary expenditures for procuring the transceivers, and making them robust enough to last 4 months of continuous use, paying for the power and space needed to make the transmissions, and the personnel for setting up and maintaining the capture. Determining the value of data is beyond the scope of this work.

So far the results have been shown in total number of observations used, but there is one more important way to look at the augmentation performance, and that there must be some foundation of capture data from which to augment. Figures 9-11 shuffle the results of the capture and augmented datasets to show the accuracy achieved on Ω_{TC} as a function of the capture data quantity that went into each model's training. This means that for a given value on the x-axis, all data points required the same number of capture observations per waveform class in order to achieve the performance shown. Obscured in these figures is the augmentation factor, or how many times each capture observation was augmented, which is upper bounded by 10 for this work due to upfront augmentation, and not online augmentation during training, with 10 being chosen due to storage constraints within the training servers. From Figures 9-11, two more beneficial aspects of augmented data can be observed. The first beneficial aspect of augmentation allows for network convergence when the number of capture observations is not substantial enough to converge on their own. This is tremendously beneficial when planning for a capture event and determining how long the event must be in order to achieve a desired performance level by establishing the trends like what was done in Table 5, but performed in an order of magnitude smaller time window as an exploratory capture event. The second benefit is seen when there are only a set number of observations available within the capture dataset, and knowledge about the degradation due to the detection algorithm, which is known, as under these conditions the accuracy of the network trained with augmentation converge, while the networks trained with capture data alone do not. From these results, while remembering that the augmentation used in this work is a static augmented dataset with a bounded number of

augmentations set to 10; the full effect of augmentation and how performance changes with dynamic, large augmentation factors (>10) and as to whether there are any diminishing returns as the augmentation factor increases is outside the scope of this work and is an area for future work.

3.3 Degradation Distribution Effect on Augmentation

The last insight offered by Figures 6-11 addresses the third question of whether knowing the distribution of the degradation is beneficial for augmentation. By contrasting the performance of Ω_{AK} , where augmentation draws from the nuisance parameter KDE, with that of Ω_{AS} , where augmentation is performed on an assumed subset of the application space, we see that having knowledge of the distributions during augmentation provides for the best performance of the network for a given set of captured data. Even just looking at the capture data on its own results in better performance as long as there is enough data available to result in a convergent network. This suggests that care should be taken when creating augmentation routines such that the distributions on the nuisance parameters are considered during the augmentation in order to achieve peak performance for a given number of capture observations. Additionally, naive methods of augmentation utilizing GANs should be cautious of developing one network capable of augmenting *any* waveform, though developing a network *per* waveform as was done in⁴¹ still might be a viable alternative to the domain knowledge approach in this work.

3.4 Results Summary

From this work, the results show that synthetic data that only considers degradations inherent in detector and isolation algorithms such as SNR, FO, and SRM, do not provide high enough fidelity data when evaluating on real-world datasets with dynamic channels. This was the case for using the assumed subset and KDE parameter draws for synthesizing the degradation, but this result should not be taken as synthetic has no value, rather just not enough value as prepared and used in this work because an increase in performance was observed in Φ_3 and Φ_5 waveform spaces with using Ω_{SK} over Ω_{SS} when only a small portion of the overall environment was considered. A stark contrast to the synthetic data was found in the value of augmentation of the dataset while only considering SNR, FO, and SRM. If the augmentation was drawn from the captured distributions observed, a mixture of increased accuracy and generalization was observed in the network's final performance on the two test sets, Ω_{TC} and Ω_{TS} . However, when augmentation was focused on a subset of the distribution regions for the same degradation types, the end resulting network saw a decrease in performance for both test sets. This shows that augmentation used properly can offer gains when taking into consideration the full range and distribution of what is expected to be observed, but naive usage could lead to performance loss instead. Both augmentation sources did have one benefit over raw capture when there was not enough of the capture data for the network to converge: in this case, both naive and KDE based augmentation can be used to provide a rough estimate how much real-world captured data

would be needed to achieve a desired performance, ignoring any asymptotic limit.

4 Future Work

New questions or efforts that can build upon these results include:

- Integration of propagation path operational requirements into dataset generation (Section 2.3.1)
- Testing the predicted quantities needed to reach 100% accuracy made by this paper with larger datasets, or identifying an asymptotic limit (Section 3.2)
- Quantifying the relationship of the augmentation factor to performance, conditionally on the amount of capture data available (Section 3.2)
- Quantifying cost of training datasets for a given RFML application (Section 3.3)
- Quantify the ability of capture data to be augmented for a different propagation path (Section 3.3)
- Incorporate the emulation of RF signal streams through channel environments that cannot be practically tested, like atmospheric scintillation⁸⁹ (Section 3.3)
- Examine the viability of generative network to perform augmentation without domain knowledge explicitly given (Section 3.4)
- Generalization of parametric training data quantification to other RFML applications (Section 3.4)

5 Conclusions

Three questions are examined and addressed within this work. First, the results tell that only considering the nuisance parameters from the detection and isolation algorithms do not provide enough to bridge the synthetic and real-world divide, and suggest that in order to bring synthetic data generation to a higher fidelity, the propagation path from DAC to ADC must be further investigated and modeled. The second question finds that while the overall quality of augmented observations are less than that of uniquely captured observations, the associated cost in terms of time and money is significantly lower with augmented data, suggesting a cost analysis can be performed to strike a balance between the two. Additionally, the use of augmentation when there is not enough data, or capturing more data is not a feasible option, allows for an increase in performance over just the captured data on its own, especially when the capture dataset is insufficient to allow for the network to converge during training. The final question is shown in the results to conclusively align with knowledge of the distributions being used while performing augmentation are consistently better than naively augmenting data with an assumed near-set parameter space. The work establishes a methodology to make a prediction for the quantity of the data needed, under all cases examined, for the number of observations needed to reach 100% accuracy in the classification problem for the provided dataset, not accounting for any asymptotic limit existing prior to reaching 100% accuracy, as well as for determining the number of observations needed to reach 95% accuracy with logistic regression when taking into consideration the asymptotic limit of the problem space.

Acknowledgements

The authors wish to thank CACI for their sponsorship of the original OTA dataset collection.

References

1. Goodfellow I, Bengio Y and Courville A. *Deep Learning*. MIT Press, 2016. <http://www.deeplearningbook.org>.
2. Nandi A and Azzouz E. Modulation recognition using artificial neural networks. *Signal Processing* 1997; 56(2): 165 – 175. DOI:[https://doi.org/10.1016/S0165-1684\(96\)00165-X](https://doi.org/10.1016/S0165-1684(96)00165-X). URL <http://www.sciencedirect.com/science/article/pii/S016516849600165X>.
3. Namjin Kim, Kehtarnavaz N, Yeary MB et al. DSP-based hierarchical neural network modulation signal classification. *IEEE Transactions on Neural Networks* 2003; 14(5): 1065–1071.
4. Fehske A, Gaedert J and Reed JH. A new approach to signal classification using spectral correlation and neural networks. In *First IEEE International Symposium on New Frontiers in Dynamic Spectrum Access Networks, 2005. DySPAN 2005*. pp. 144–150. DOI:10.1109/DYSPAN.2005.1542629.
5. Mody AN, Blatt SR, Mills DG et al. Recent advances in cognitive communications. *IEEE Communications Magazine* 2007; 45(10): 54–61. DOI:10.1109/MCOM.2007.4342823.
6. Ge F, Chen Q, Wang Y et al. Cognitive radio: From spectrum sharing to adaptive learning and reconfiguration. In *2008 IEEE Aerospace Conference*. pp. 1–10. DOI:10.1109/AERO.2008.4526372.
7. Bixio L, Ottonello M, Sallam H et al. Signal classification based on spectral redundancy and neural network ensembles. In *2009 4th International Conference on Cognitive Radio Oriented Wireless Networks and Communications*. pp. 1–6. DOI:10.1109/CROWNCOM.2009.5189036.
8. Clancy TC and Khawar A. Security threats to signal classifiers using self-organizing maps. In *2009 4th International Conference on Cognitive Radio Oriented Wireless Networks and Communications*. pp. 1–6. DOI:10.1109/CROWNCOM.2009.5189050.
9. Ramón MM, Atwood T, Barbin S et al. Signal classification with an SVM-FFT approach for feature extraction in cognitive radio. In *2009 SBMO/IEEE MTT-S International Microwave and Optoelectronics Conference (IMOC)*. pp. 286–289. DOI: 10.1109/IMOC.2009.5427579.
10. Popoola JJ and v Olst R. A novel modulation-sensing method. *IEEE Vehicular Technology Magazine* 2011; 6(3): 60–69. DOI: 10.1109/MVT.2011.941893.
11. Shan Kang, Naiwen Chen, Mi Yan et al. Detecting identity-spoof attack based on bp network in cognitive radio network. In *Proceedings of 2011 Cross Strait Quad-Regional Radio Science and Wireless Technology Conference*, volume 2. pp. 1603–1606. DOI:10.1109/CSQRWC.2011.6037280.
12. Pu D and Wyglinski AM. Primary user emulation detection using frequency domain action recognition. In *Proceedings of 2011 IEEE Pacific Rim Conference on Communications, Computers and Signal Processing*. pp. 791–796. DOI:10.1109/PACRIM.2011.6032995.
13. He F, Xu X, Zhou L et al. A learning based cognitive radio receiver. In *2011 - MILCOM 2011 Military Communications Conference*. pp. 7–12. DOI:10.1109/MILCOM.2011.6127675.

14. Abdelreheem MMT and Helmi MO. Digital modulation classification through time and frequency domain features using neural networks. In *2012 IX International Symposium on Telecommunications (BIHTEL)*. pp. 1–5. DOI:10.1109/BIHTEL.2012.6412073.
15. Li S, Wang X and Wang J. Manifold learning-based automatic signal identification in cognitive radio networks. *IET Communications* 2012; 6(8): 955–963. DOI:10.1049/iet-com.2010.0590.
16. Thilina KM, Choi KW, Saquib N et al. Machine learning techniques for cooperative spectrum sensing in cognitive radio networks. *IEEE Journal on Selected Areas in Communications* 2013; 31(11): 2209–2221. DOI:10.1109/JSAC.2013.131120.
17. Popoola JJ and van Olst R. The performance evaluation of a spectrum sensing implementation using an automatic modulation classification detection method with a universal software radio peripheral. *Expert Systems with Applications* 2013; 40(6): 2165 – 2173. DOI:<https://doi.org/10.1016/j.eswa.2012.10.047>. URL <http://www.sciencedirect.com/science/article/pii/S0957417412011712>.
18. Kim S and Giannakis GB. Dynamic learning for cognitive radio sensing. In *2013 5th IEEE International Workshop on Computational Advances in Multi-Sensor Adaptive Processing (CAMSAP)*. pp. 388–391. DOI:10.1109/CAMSAP.2013.6714089.
19. Tsakmalis A, Chatzinotas S and Ottersten B. Automatic modulation classification for adaptive power control in cognitive satellite communications. In *2014 7th Advanced Satellite Multimedia Systems Conference and the 13th Signal Processing for Space Communications Workshop (ASMS/SPSC)*. pp. 234–240. DOI:10.1109/ASMS-SPSC.2014.6934549.
20. Chen T, Liu J, Xiao L et al. Anti-jamming transmissions with learning in heterogenous cognitive radio networks. In *2015 IEEE Wireless Communications and Networking Conference Workshops (WCNCW)*. pp. 293–298. DOI:10.1109/WCNCW.2015.7122570.
21. Mendis GJ, Wei J and Madanayake A. Deep learning-based automated modulation classification for cognitive radio. In *2016 IEEE International Conference on Communication Systems (ICCS)*. pp. 1–6. DOI:10.1109/ICCS.2016.7833571.
22. O’Shea TJ, Pemula L, Batra D et al. Radio transformer networks: Attention models for learning to synchronize in wireless systems. In *2016 50th Asilomar Conference on Signals, Systems and Computers*. pp. 662–666. DOI:10.1109/ACSSC.2016.7869126.
23. O’Shea TJ, Hitefield S and Corgan J. End-to-end radio traffic sequence recognition with recurrent neural networks. In *2016 IEEE Global Conference on Signal and Information Processing (GlobalSIP)*. pp. 277–281. DOI:10.1109/GlobalSIP.2016.7905847.
24. O’Shea T and West N. Radio machine learning dataset generation with GNU radio. *Proceedings of the GNU Radio Conference* 2016; 1(1). URL <https://pubs.gnuradio.org/index.php/grcon/article/view/11>.
25. O’Shea TJ, Corgan J and Clancy TC. Convolutional Radio Modulation Recognition Networks. *arXiv e-prints* 2016; : arXiv:1602.041051602.04105.
26. West NE, Harwell K and McCall B. DFT signal detection and channelization with a deep neural network modulation classifier. In *2017 IEEE International Symposium on Dynamic Spectrum Access Networks (DySPAN)*. pp. 1–3. DOI:10.1109/DySPAN.2017.7920745.
27. West NE and O’Shea T. Deep architectures for modulation recognition. In *2017 IEEE International Symposium on Dynamic Spectrum Access Networks (DySPAN)*. pp. 1–6. DOI: 10.1109/DySPAN.2017.7920754.
28. Karra K, Kuzdeba S and Petersen J. Modulation recognition using hierarchical deep neural networks. In *2017 IEEE International Symposium on Dynamic Spectrum Access Networks (DySPAN)*. pp. 1–3. DOI:10.1109/DySPAN.2017.7920746.
29. O’Shea T, Roy T and Clancy TC. Learning robust general radio signal detection using computer vision methods. In *2017 51st Asilomar Conference on Signals, Systems, and Computers*. pp. 829–832.
30. Peng S, Jiang H, Wang H et al. Modulation classification using convolutional neural network based deep learning model. In *2017 26th Wireless and Optical Communication Conference (WOCC)*. pp. 1–5. DOI:10.1109/WOCC.2017.7929000.
31. Reddy KPK, Yeleswarapu Y and Darak SJ. Performance evaluation of cumulant feature based automatic modulation classifier on USRP testbed. In *2017 9th International Conference on Communication Systems and Networks (COMSNETS)*. pp. 393–394. DOI:10.1109/COMSNETS.2017.7945409.
32. Nawaz T, Marcenaro L and Regazzoni CS. Stealthy jammer detection algorithm for wide-band radios: A physical layer approach. In *2017 IEEE 13th International Conference on Wireless and Mobile Computing, Networking and Communications (WiMob)*. pp. 79–83. DOI:10.1109/WiMOB.2017.8115792.
33. Nawaz T, Marcenaro L and Regazzoni CS. Cyclostationary-based jammer detection for wideband radios using compressed sensing and artificial neural network. *International Journal of Distributed Sensor Networks* 2017; 13(12): 1. URL <http://login.ezproxy.lib.vt.edu/login?url=http://search.ebscohost.com/login.aspx?direct=true&db=iih&AN=127039926&scope=site>.
34. Ambaw AB, Bari M and Doroslovački M. A case for stacked autoencoder based order recognition of continuous-phase FSK. In *2017 51st Annual Conference on Information Sciences and Systems (CISS)*. pp. 1–6. DOI:10.1109/CISS.2017.7926151.
35. Ali A, Yangyu F and Liu S. Automatic modulation classification of digital modulation signals with stacked autoencoders. *Digital Signal Processing* 2017; 71: 108 – 116. DOI:<https://doi.org/10.1016/j.dsp.2017.09.005>. URL <http://www.sciencedirect.com/science/article/pii/S1051200417302087>.
36. Hong D, Zhang Z and Xu X. Automatic modulation classification using recurrent neural networks. In *2017 3rd IEEE International Conference on Computer and Communications (ICCC)*. pp. 695–700. DOI:10.1109/CompComm.2017.8322633.
37. Yelalwar RG and Ravinder Y. Artificial neural network based approach for spectrum sensing in cognitive radio. In *2018 International Conference on Wireless Communications, Signal Processing and Networking (WiSPNET)*. pp. 1–5. DOI:10.1109/WiSPNET.2018.8538729.
38. Hauser SC, Headley WC and Michaels AJ. Signal detection effects on deep neural networks utilizing raw IQ for modulation classification. In *MILCOM 2017 - 2017 IEEE Military*

- Communications Conference (MILCOM)*. pp. 121–127. DOI: 10.1109/MILCOM.2017.8170853.
39. Hiremath SM, Deshmukh S, Rakesh R et al. Blind identification of radio access techniques based on time-frequency analysis and convolutional neural network. In *TENCON 2018 - 2018 IEEE Region 10 Conference*. pp. 1163–1167. DOI:10.1109/TENCON.2018.8650355.
 40. Tang B, Tu Y, Zhang Z et al. Digital signal modulation classification with data augmentation using generative adversarial nets in cognitive radio networks. *IEEE Access* 2018; 6: 15713–15722. DOI:10.1109/ACCESS.2018.2815741.
 41. Davaslioglu K and Sagduyu YE. Generative adversarial learning for spectrum sensing. In *2018 IEEE International Conference on Communications (ICC)*. pp. 1–6. DOI:10.1109/ICC.2018.8422223.
 42. Kulin M, Kazaz T, Moerman I et al. End-to-end learning from spectrum data: A deep learning approach for wireless signal identification in spectrum monitoring applications. *IEEE Access* 2018; 6: 18484–18501. DOI:10.1109/ACCESS.2018.2818794.
 43. Wu Y, Li X and Fang J. A deep learning approach for modulation recognition via exploiting temporal correlations. In *2018 IEEE 19th International Workshop on Signal Processing Advances in Wireless Communications (SPAWC)*. pp. 1–5. DOI:10.1109/SPAWC.2018.8445938.
 44. Li Z, Liu R, Lin X et al. Detection of frequency-hopping signals based on deep neural networks. In *2018 IEEE 3rd International Conference on Communication and Information Systems (ICCIS)*. pp. 49–52. DOI:10.1109/ICOMIS.2018.8645029.
 45. Tandiya N, Jauhar A, Marojevic V et al. Deep predictive coding neural network for RF anomaly detection in wireless networks. In *2018 IEEE International Conference on Communications Workshops (ICC Workshops)*. pp. 1–6. DOI:10.1109/ICCW.2018.8403654.
 46. Subekti A, Pardede HF, Sustika R et al. Spectrum sensing for cognitive radio using deep autoencoder neural network and SVM. In *2018 International Conference on Radar, Antenna, Microwave, Electronics, and Telecommunications (ICRAMET)*. pp. 81–85. DOI:10.1109/ICRAMET.2018.8683930.
 47. Jayaweera SK and Aref MA. Cognitive engine design for spectrum situational awareness and signals intelligence. In *2018 21st International Symposium on Wireless Personal Multimedia Communications (WPMC)*. pp. 478–483. DOI: 10.1109/WPMC.2018.8712936.
 48. O’Shea TJ, Roy T and Clancy TC. Over-the-air deep learning based radio signal classification. *IEEE Journal of Selected Topics in Signal Processing* 2018; 12(1): 168–179.
 49. ZHANG Y, LIU T, ZHANG L et al. A deep learning approach for modulation recognition. In *2018 IEEE 23rd International Conference on Digital Signal Processing (DSP)*. pp. 1–5. DOI: 10.1109/ICDSP.2018.8631811.
 50. Sang Y and Li LA. Application of novel architectures for modulation recognition. In *2018 IEEE Asia Pacific Conference on Circuits and Systems (APCCAS)*. pp. 159–162. DOI:10.1109/APCCAS.2018.8605691.
 51. Vanhoy G, Thurston N, Burger A et al. Hierarchical modulation classification using deep learning. In *MILCOM 2018 - 2018 IEEE Military Communications Conference (MILCOM)*. pp. 20–25. DOI:10.1109/MILCOM.2018.8599861.
 52. Shapero SA, Dill AB and Odelowo BO. Identifying agile waveforms with neural networks. In *2018 21st International Conference on Information Fusion (FUSION)*. pp. 745–752. DOI:10.23919/ICIF.2018.8455370.
 53. Yashashwi K, Sethi A and Chaporkar P. A learnable distortion correction module for modulation recognition. *IEEE Wireless Communications Letters* 2019; 8(1): 77–80. DOI:10.1109/LWC.2018.2855749.
 54. Peng S, Jiang H, Wang H et al. Modulation classification based on signal constellation diagrams and deep learning. *IEEE Transactions on Neural Networks and Learning Systems* 2019; 30(3): 718–727. DOI:10.1109/TNNLS.2018.2850703.
 55. Wang Y, Liu M, Yang J et al. Data-driven deep learning for automatic modulation recognition in cognitive radios. *IEEE Transactions on Vehicular Technology* 2019; 68(4): 4074–4077. DOI:10.1109/TVT.2019.2900460.
 56. Liu H, Zhu X and Fujii T. Cyclostationary based full-duplex spectrum sensing using adversarial training for convolutional neural networks. In *2019 International Conference on Artificial Intelligence in Information and Communication (ICAIIIC)*. pp. 369–374. DOI:10.1109/ICAIIIC.2019.8669026.
 57. Zheng S, Qi P, Chen S et al. Fusion methods for CNN-based automatic modulation classification. *IEEE Access* 2019; 7: 66496–66504. DOI:10.1109/ACCESS.2019.2918136.
 58. Wang P and Vindiola M. Data augmentation for blind signal classification. In *MILCOM 2019 - 2019 IEEE Military Communications Conference (MILCOM)*. pp. 149–154.
 59. Clark WH, Arndorfer V, Tamir B et al. Developing RFML intuition: An automatic modulation classification architecture case study. In *MILCOM 2019 - 2019 IEEE Military Communications Conference (MILCOM)*. pp. 136–142.
 60. Wong LJ, Headley WC and Michaels AJ. Specific emitter identification using convolutional neural network-based IQ imbalance estimators. *IEEE Access* 2019; 7: 33544–33555.
 61. Merchant K and Nousain B. Toward receiver-agnostic RF fingerprint verification. In *2019 IEEE Globecom Workshops (GC Wkshps)*. pp. 1–6.
 62. Cai Q, Chen S, Li X et al. An integrated incremental self-organizing map and hierarchical neural network approach for cognitive radio learning. In *The 2010 International Joint Conference on Neural Networks (IJCNN)*. pp. 1–6. DOI: 10.1109/IJCNN.2010.5596337.
 63. Torres-Sospedra J, Montoliu R, Martínez-Usó A et al. UJIIndoorLoc: A new multi-building and multi-floor database for WLAN fingerprint-based indoor localization problems. In *2014 International Conference on Indoor Positioning and Indoor Navigation (IPIN)*. pp. 261–270.
 64. Kumar KAA. SoC implementation of a modulation classification module for cognitive radios. In *2016 International Conference on Communication Systems and Networks (ComNet)*. pp. 87–92. DOI:10.1109/CSN.2016.7823992.
 65. Schmidt M, Block D and Meier U. Wireless interference identification with convolutional neural networks. In *2017 IEEE 15th International Conference on Industrial Informatics (INDIN)*. pp. 180–185. DOI:10.1109/INDIN.2017.8104767.
 66. Vyas MR, Patel DK and Lopez-Benitez M. Artificial neural network based hybrid spectrum sensing scheme for cognitive radio. In *2017 IEEE 28th Annual International Symposium on Personal, Indoor, and Mobile Radio Communications (PIMRC)*. pp. 1–7. DOI:10.1109/PIMRC.2017.8292449.

67. Bitar N, Muhammad S and Refai HH. Wireless technology identification using deep convolutional neural networks. In *2017 IEEE 28th Annual International Symposium on Personal, Indoor, and Mobile Radio Communications (PIMRC)*. pp. 1–6. DOI:10.1109/PIMRC.2017.8292183.
68. O’Shea TJ, Roy T and Erpek T. Spectral detection and localization of radio events with learned convolutional neural features. In *2017 25th European Signal Processing Conference (EUSIPCO)*. pp. 331–335.
69. Fernandes SS, Makiuchi MR, Lamar MV et al. An adaptive recurrent neural network model dedicated to opportunistic communication in wireless networks. In *2018 International Joint Conference on Neural Networks (IJCNN)*. pp. 01–08. DOI:10.1109/IJCNN.2018.8489720.
70. Testi E, Favarelli E and Giorgetti A. Machine learning for user traffic classification in wireless systems. In *2018 26th European Signal Processing Conference (EUSIPCO)*. pp. 2040–2044. DOI:10.23919/EUSIPCO.2018.8553196.
71. Yi S, Wang H, Xue W et al. Interference source identification for IEEE 802.15.4 wireless sensor networks using deep learning. In *2018 IEEE 29th Annual International Symposium on Personal, Indoor and Mobile Radio Communications (PIMRC)*. pp. 1–7. DOI:10.1109/PIMRC.2018.8580857.
72. Merchant K, Revay S, Stantchev G et al. Deep learning for RF device fingerprinting in cognitive communication networks. *IEEE Journal of Selected Topics in Signal Processing* 2018; 12(1): 160–167. DOI:10.1109/JSTSP.2018.2796446.
73. Wong LJ, Headley WC, Andrews S et al. Clustering learned CNN features from raw I/Q data for emitter identification. In *MILCOM 2018 - 2018 IEEE Military Communications Conference (MILCOM)*. pp. 26–33. DOI:10.1109/MILCOM.2018.8599847.
74. Mohammed S, El Abdessamad R, Saadane R et al. Performance evaluation of spectrum sensing implementation using artificial neural networks and energy detection method. In *2018 International Conference on Electronics, Control, Optimization and Computer Science (ICECOCS)*. pp. 1–6. DOI:10.1109/ICECOCS.2018.8610506.
75. Elbakly R, Aly H and Youssef M. TrueStory: Accurate and robust RF-based floor estimation for challenging indoor environments. *IEEE Sensors Journal* 2018; 18(24): 10115–10124.
76. Mendis GJ, Wei J and Madanayake A. Deep learning based radio-signal identification with hardware design. *IEEE Transactions on Aerospace and Electronic Systems* 2019; : 1–1 DOI:10.1109/TAES.2019.2891155.
77. Hiremath SM, Behura S, Kedia S et al. Deep learning-based modulation classification using time and Stockwell domain channeling. In *2019 National Conference on Communications (NCC)*. pp. 1–6. DOI:10.1109/NCC.2019.8732258.
78. Sankhe K, Belgiovine M, Zhou F et al. Oracle: Optimized radio classification through convolutional neural networks. In *IEEE INFOCOM 2019-IEEE Conference on Computer Communications*. IEEE, pp. 370–378.
79. AlHajri MI, Ali NT and Shubair RM. Indoor localization for IoT using adaptive feature selection: A cascaded machine learning approach. *IEEE Antennas and Wireless Propagation Letters* 2019; 18(11): 2306–2310.
80. Chawathe SS. Indoor-location classification using RF signatures. In *2019 IEEE 18th International Symposium on Network Computing and Applications (NCA)*. pp. 1–4.
81. Merchant K and Nousain B. Enhanced RF fingerprinting for IoT devices with recurrent neural networks. In *MILCOM 2019 - 2019 IEEE Military Communications Conference (MILCOM)*. pp. 590–597.
82. Simard PY, Steinkraus D and Platt JC. Best practices for convolutional neural networks applied to visual document analysis. In *Seventh International Conference on Document Analysis and Recognition, 2003. Proceedings*. pp. 958–963. DOI:10.1109/ICDAR.2003.1227801.
83. Krizhevsky A, Sutskever I and Hinton GE. Imagenet classification with deep convolutional neural networks. In Pereira F, Burges CJC, Bottou L et al. (eds.) *Advances in Neural Information Processing Systems 25*. Curran Associates, Inc., 2012. pp. 1097–1105.
84. Yaeger LS, Lyon RF and Webb BJ. Effective training of a neural network character classifier for word recognition. In Mozer MC, Jordan MI and Petsche T (eds.) *Advances in Neural Information Processing Systems 9*. MIT Press, 1997. pp. 807–816.
85. Flowers B and Headley WC. Adversarial radio frequency machine learning (RFML) with PyTorch, 2019.
86. Kingma DP and Ba JL. Adam: A method for stochastic optimization. San Diego, CA, United states.
87. Swami A and Sadler B. Hierarchical digital modulation classification using cumulants. *Communications, IEEE Transactions on* 2000; 48(3): 416–429. DOI:10.1109/26.837045.
88. Welch BL. The generalization of student’s’ problem when several different population variances are involved. *Biometrika* 1947; 34(1/2): 28–35.
89. Sward W, Swanson T and Williams M. Scintillation simulator test results: Hardware-in-the-loop emulation of ionospheric scintillation. In *2014 IEEE Military Communications Conference*. pp. 1361–1367.